

Hidden subsystem symmetry protected states in competing topological orders

Shi Feng*

Department of Physics, The Ohio State University, Columbus, Ohio 43210, USA

(Dated: September 6, 2023)

We reveal the connection between two-dimensional subsystem symmetry-protected topological (SSPT) states and two-dimensional topological orders via a self-dual frustrated toric code model. This model, an enrichment of the toric code (TC) with its dual interactions, can be mapped to a model defined on the dual lattice with subsystem symmetries and subextensive ground state degeneracy. The map connects exactly the frustrated TC to two copies of the topological plaquette Ising model (TPIM), as a strong SSPT model with linear subsystem symmetries. The membrane order parameter of TPIM is exactly mapped to dual TC stabilizers as the order parameter of the frustrated TC model, and the transition between the SSPT-ordered TPIM to the trivial paramagnetic phase is mapped to the transition between two distinct topological orders. We also demonstrate that this picture of frustrated TC can be used to construct other SSPT models, hinting at a subtle linkage between SSPT order and topological order in two dimensions.

The exploration of topological phases of matter has expanded our understanding of distinct states of matter beyond those conventionally defined by spontaneously broken symmetry. Three primary categories of topological phases have emerged: (1) Phases protected by an unbroken global symmetry, i.e. symmetry protected topological (SPT) phases exemplified by topological band insulators [1] and integer spin chains [2, 3]. (2) Topologically ordered phases [4, 5], as found in matters like quantum spin liquids [6–8], Kitaev’s toric code [9], and fractional quantum Hall systems [10], known for their inherent or emergent local gauge fields and braiding statistics. (3) The most recent and compelling addition, the Subsystem Symmetry Protected Topological (SSPT) phases [11, 12], which lies at an intermediate position between the first two categories, featuring a sub-global symmetry and non-local order parameter. Just as SPT states are known for boundary modes that are protected by global symmetries, SSPT states are also protected in a similar fashion, but by their subextensive subsystem symmetries. Such phases introduce new forms of matter characterized by subextensive topological ground-state degeneracy (GSD), quasiparticle excitations with fractonic mobility [13–16].

The primary objective of this paper is to elucidate the intricate relationship between 2D SSPT states and 2D topological order. We concentrate on the “strong SSPT” states [11, 12], distinct from the “weak SSPT” states in that they cannot be simply regarded as decoupled or weakly coupled SPT states in lower dimensions. While several related scenarios are well-understood, such as the connection between 2D global SPT orders and their dual 2D topological orders [18, 19], and between 3D SSPT orders and 3D fracton orders [20, 21], the relationship between 2D SSPT orders and 2D topological orders remains relatively less explored. In this work, drawing parallels with the hidden symmetry-breaking picture observed in an SPT phase after a non-local transformation [22, 23], we demonstrate the existence of hidden competing topological orders within 2D SSPT phases, or con-

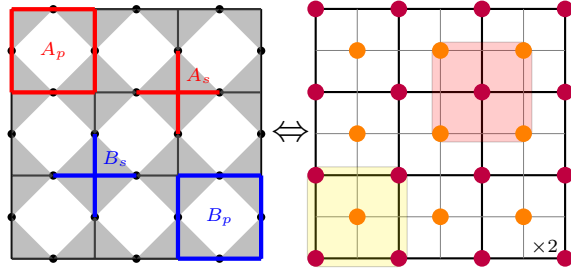


FIG. 1. Mapping between the self-dual frustrated TC model (Left) and two copies of TPIM (Right). Left: TC square lattice A in solid black lines, where qubits live on links; its equivalence in terms of checker-board lattice in Wen’s plaquette representation [17] – star operator corresponds to shaded square while plaquette operator to white square; and TC stabilizers A_s (red star), B_p (blue plaquette), and dual TC stabilizers A_p (red plaquette) and B_s (blue star). Right: The TPIM lattice. Two sublattices are denoted by black and gray lines, with qubits labelled in orange and purple. The two five-qubit interactions: $\sigma_{\text{center}}^z \prod_{i \in \text{corners}} \sigma_i^x$, are circled in yellow and red.

versely, the hidden 2D SSPT phases within competing 2D topological orders. We note that previous studies have established a connection between the SSPT triangular cluster-state model and its dual topological order via the Xu-Moore duality [20, 24], we here take a different approach: by using a non-local map to relate the simplest topological order, the toric code (TC), to the simplest strong SSPT model, the topological plaquette Ising model (TPIM) [Fig. 1].

Motivated by the self-duality of TPIM [12], it is natural to start from a manifestly self-dual model with topological order, though later we will show that half of it suffices to give a similar picture. Let us consider the following self-dual frustrated TC Hamiltonian (FTC), where we superimpose the TC interactions with its dual interactions

$$H_{\text{FTC}} = - \left[\sum_s A_s + \sum_p B_p \right] - \alpha \left[\sum_p A_p + \sum_s B_s \right] \quad (1)$$

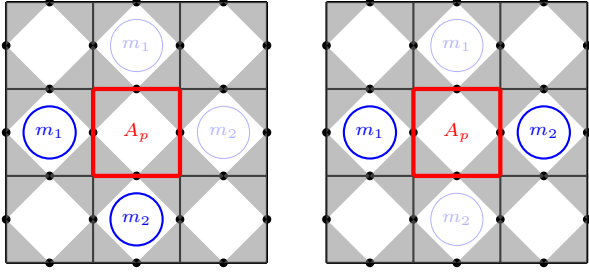


FIG. 2. The anyon mobility analysis in leading order perturbation theory. Left: A local perturbation by the dual TC operator A_p (in red) moves the two anyon bound state $m_1 \times m_2$ aligned in diagonal direction (deep blue) to its adjacent position (faint blue) along the off-diagonal direction, resulting in a bound-state dispersion along the one-dimensional direction. Right: The same perturbation transitions the horizontally aligned two-anyon bound state (deep blue) to a vertically aligned state (faint blue), and conversely. This results in a stable, immobile bound state.

The first two terms, $A_s = \prod_{i \in s} \sigma_i^x$, $B_p = \prod_{i \in p} \sigma_i^z$, are the X and Z parity checks in the canonical H_{TC} of TC, while the dual interactions, $A_p = \prod_{i \in p} \sigma_i^x$, $B_s = \prod_{i \in s} \sigma_i^z$ in the later two terms, are added as perturbations parameterized by α . It depicts the competition between two mutually frustrating TCs and enjoys a duality $\alpha \leftrightarrow \alpha^{-1}$. At transition $\alpha = 1$ both vertices and plaquettes play the same role. Note this is different from the 3D fracton orders, which typically involve stacking 2D toric codes to realize higher-dimensional fracton phases [16, 25, 26]. Here the perturbation is not disjoint from the original 2D TC and it does not commute with H_{TC} , e.g. the dual operator A_p and its neighboring plaquette $B_{p'}$ share a single link. The original toric code has finite number of GSD, however, we will show that the two competing TCs in Eq. 1 can be mapped to a model with a subextensively infinite number of degenerate ground states, which is intimately related to SSPT states and linear symmetries that play a central role in 2D fractonic physics [14, 15, 27].

Fractonic anyons:- A common signature of the emergence of subsystem symmetries is the effective dimensional reduction, i.e. the fractonic nature, of excitations [14, 27, 28]. Here we start from the mobility of anyons in the leading order perturbation theory as a rudimentary indicator, showing that the competition between the two Z_2 topological orders give rise to fractonic behaviors in 2D. Note that none of the two terms in the perturbation of Eq. 1 can create a pair of anyon, so fractonic behavior is expected. At $\alpha = 0$, the TC model has four types of Abelian anyons: $1, e, m, \epsilon = e \times m$, where e and m are electric charge and magnetic flux in the context of Z_2 gauge theory, behaving as self bosons and mutual semions; while the $e \times m$ bound state ϵ have fermionic statistics. The ground state is an anyon vacuum, elementary excitations under open boundary condition can be any one of the e, m or $e \times m$ anyons. It is natural

to ask what is the dynamics of these elementary particles under an $\alpha \neq 0$ perturbation. Indeed, it is known that the TC, when perturbed by a transverse field $\sum_i \sigma_i^x$ or $\sum_i \sigma_i^z$ [29–31], a single e and single m anyons would disperse isotropically; and by $\sum_i \sigma_i^y$ the fermionic ϵ particles would disperse linearly [32, 33]. However, it is clear from the leading order perturbation that in the case of Eq. 1, none of these particles would gain mobility; while it is the anyon bound states, e.g. the two bosonic bound states, $e_1 \times e_2$ or $m_1 \times m_2$ with individual anyons aligned in (off)diagonal direction, that develop partially mobile softened modes. The subscript is used to emphasize that they are spacially separated with a lattice constant and do not fuse to a trivial state. It is readily to see that these particles, while mobile, enjoys only a constraint mobility. For example, a bound state created to be aligned with diagonal direction can only move along the off-diagonal direction, as shown in Fig. 2(left). Nevertheless, the bound state created in vertical or horizontal directions remains stable, as shown in Fig. 2(right). To the leading order perturbation theory, its effective dispersion can be described by

$$\varepsilon_{m_1 \times m_2}(\mathbf{k}) = \varepsilon_{e_1 \times e_2}(\mathbf{k}) = 4 - 2 \cos(\mathbf{k} \cdot \mathbf{d}) \quad (2)$$

with \mathbf{d} in the diagonal or off-diagonal direction. Hence the two-anyon bound state does not condense at the transition $\alpha = 1$, indeed, the phase transition is instead driven by the four-anyon bound state, which is free to move in all directions. These properties are similar to the 2D fractonic property of the plaquette Ising model (PIM) where four-spin-flip excitation can move without constraint; while single- or two-spin-flip excitations are either immobile or partially mobile along lines [14, 33].

Order parameter:- For the ground state property of Eq. 1 without anyon excitations, we also define the topological order parameter. In the large- α limit, a vacuum state of the dual anyons, i.e. A_p and B_s in the other set of TC stabilizers, are guaranteed at ground state by duality. Naturally, we can use these operators, or their product in some (potentially disconnected) region \mathcal{M} , as topological order parameters:

$$O_p = \left\langle \prod_{p \in \mathcal{M}} A_p \right\rangle, \quad O_s = \left\langle \prod_{s \in \mathcal{M}} B_s \right\rangle \quad (3)$$

such that the phase of $\alpha < (>)1$ corresponds to $O = 0(1)$. Here we restrict ourselves to open boundary condition, ruling out the non-contractible Wilson loops for convenience. For the smallest \mathcal{M} , the order parameter reduces to a single star A_p or plaquette B_s .

Map to TPIM:- Let us now introduce a new set of spin variables living on the vertices and faces of the dual lattice $\tilde{\Lambda}$ [33, 34], where new degrees of freedom are denoted by hollow squares in Fig. 3(a). We apply a non-local transformation, relating a pauli matrix $\tilde{\sigma}_x$ on the

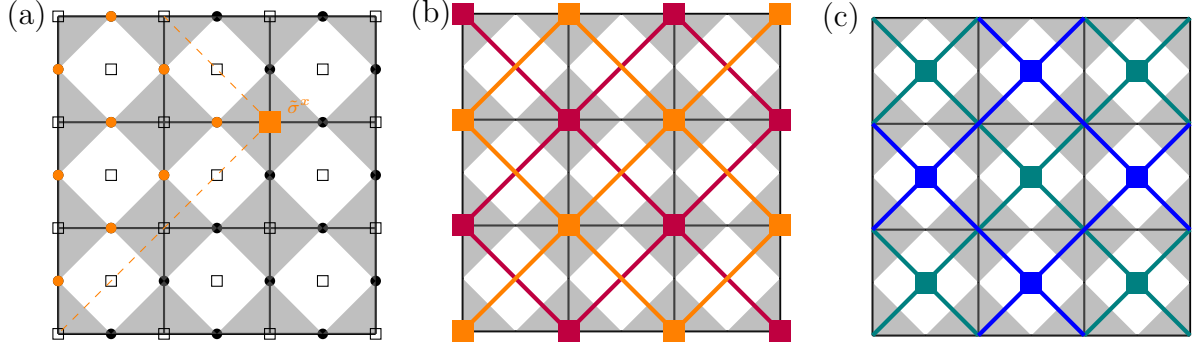


FIG. 3. (a) An illustration of the transformation in Eq. 4. Qubits in Λ lattice are denoted by filled dots, while qubits in the dual lattice $\tilde{\Lambda}$ are denoted by hollow squares. In Eq. 4, the non-local transformation relates a qubit in $\tilde{\Lambda}$ (represented by the orange square) to the set of qubits in Λ (denoted by the orange dots) that are located within the dashed triangular region immediately to its left (thus the symbol $>$). (b,c) Two copies of TPIM in the dual lattices after the transformation of FTC. (b) One copy of TPIM is defined on vertices in $\tilde{\Lambda}$, denoted by V . The two emergent sublattices $V_1, V_2 \in V$ are denoted by filled orange and red squares, corresponding to the two sublattices shown in Fig. 1(right). (c) The second TPIM copy defined on centers of the faces in $\tilde{\Lambda}$, denoted by F . The two emergent sublattices $F_1, F_2 \in F$ are labelled by filled green and blue squares.

dual lattice to a set of qubits on the original lattice, and identify $\tilde{\sigma}^z$ as stabilizer operators:

$$\tilde{\sigma}_j^x = \prod_{i>j} \sigma_i^y, \quad \tilde{\sigma}_{j(s)}^z = A_s, \quad \tilde{\sigma}_{j(p)}^z = B_p \quad (4)$$

as is illustrated in Fig. 3(a), $\tilde{\sigma}_j^x$ on the dual lattice (orange square) is given by the product of σ_i^y on the original lattice (orange dots). It is readily to check that it is a faithful representation that respects Pauli algebra. Under this mapping, one copy of the TC can be treated as trivial Ising variables, while the other is responsible for all emerging non-trivial properties. For clarity, let us first rewrite the operators of the dual TC, B_s and A_p , in terms of the original TC variables:

$$B_s = A_s \prod_{i \in s} \sigma_i^y, \quad A_p = \prod_{i \in p} \sigma_i^y B_p \quad (5)$$

by the identity $\sigma^a \sigma^b = \delta_{ab} + i\epsilon^{abc} \sigma^c$. In terms of $\tilde{\sigma}^x$ and $\tilde{\sigma}^z$ defined in Eq. 4, they can be written into:

$$B_s = \tilde{\sigma}_{c(\tilde{p}_V)}^z \prod_{i \in \tilde{p}_V} \tilde{\sigma}_i^x, \quad A_p = \tilde{\sigma}_{c(\tilde{p}_F)}^z \prod_{i \in \tilde{p}_F} \tilde{\sigma}_i^x \quad (6)$$

Here \tilde{p}_V denotes a plaquette defined on the vertices of the dual lattice $\tilde{\Lambda}$ that encloses one vertex in $\tilde{\Lambda}$, as illustrated in Fig. 3(b), where the enclosed qubit and the qubits of the plaquette live in different emergent sublattices, colored by orange and purple squares. \tilde{p}_F denotes a plaquette defined on face centers of $\tilde{\Lambda}$ that encloses another face center in $\tilde{\Lambda}$, as illustrated in Fig. 3(c). Again the enclosed qubit and the qubits of the plaquette live in different emergent sublattices, colored by green and blue squares. $c(\tilde{p}_V)$ denotes the site that lies at the center of a vertex-plaquette, while $c(\tilde{p}_F)$ denotes that of a face-center plaquette. After this mapping, it is readily to

see that the FTC amounts to adding up interactions in $V, F \in \tilde{\Lambda}$:

$$\mathcal{H}_\eta = -\alpha \sum_{c(\tilde{p}_\eta)} \tilde{\sigma}_{c(\tilde{p}_\eta)}^z \prod_{i \in \tilde{p}_\eta} \tilde{\sigma}_i^x - \sum_{c(\tilde{p}_\eta)} \tilde{\sigma}_{c(\tilde{p}_\eta)}^z, \quad \eta = V, F \quad (7)$$

where each η , represented in Fig. 3(b) or (c), corresponds to one copy of TPIM. We use the calligraphic \mathcal{H} to remind the reader that it is one of the two disjoint TPIM Hamiltonians. Eq. 7 is equivalent to the TPIM (or cluster-state model) protected by a subextensive number of $Z_2 \times Z_2$ linear symmetries. For $\alpha < 1$, Eq. 7 reduces to Ising paramagnet in $\tilde{\Lambda}$ which is equivalent to a TC; while when $\alpha > 1$ the system becomes strong SSPT state. For each copy, e.g. one defined on the V lattice, the symmetry generators are given by:

$$U_m^{V_i} = \prod_{n \in \text{cols}} \tilde{\sigma}_{m,n}^z, \quad U_n^{V_i} = \prod_{m \in \text{rows}} \tilde{\sigma}_{m,n}^z \quad (8)$$

The notation $U_{m(n)}^{V_i}$ stands for the linear unitary operators defined on each row (column) inside the emergent sublattice V_i , where $i = 1, 2$ corresponds to the purple and orange sites in Fig. 3(b), and the m, n labels the rows and columns of V_i . Assume the original lattice Λ is of the size $2L_x \times 2L_y$, Eq. 7 describes two copies of TPIM model, with each defined on a $L_x \times L_y$ sublattice having

$$\text{GSD}_{V(F)} = 4^{L_x + L_y - 1} \quad (9)$$

corresponding to the subextensive $Z_2 \times Z_2$ symmetry-protected edge modes of TPIM. Indeed, one may choose to perturb the TC Hamiltonian only by either one of A_p or B_s to get only one copy of the TPIM, and a lattice of $L_x \times L_y$ would give the same GSD. In fact, a closer inspection of Eq. 6 and Eq. 7 readily reveals that a single

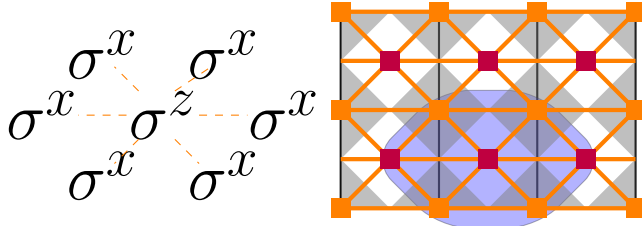


FIG. 4. The triangular cluster model with SSPT order. The generator of the SSPT model is the seven-point interaction shown on the left side and the blue shadow on the right side. It can be mapped onto a frustrated 2D TC model defined in Eq. 12, whereby a triangular lattice in the dual lattice merge. Here for clarity we label the face-centered sites of $\tilde{\Lambda}$ in red, and vertex sites of $\tilde{\Lambda}$ in orange.

TPIM can emerge from a half of the FTC, whereby only one of V or F sublattices emerge:

$$-\sum_s (A_s + \alpha B_s) \cong -\sum_p (B_p + \alpha A_p) \mapsto H_{\text{TPIM}} \quad (10)$$

In this form the perturbation analysis of anyon mobility is no longer viable, however, it helps in singling out a minimal stabilizer model that is mappable to a strong SSPT-ordered TPIM in Eq. 7.

Given the correspondence between SSPT states and the FTC model, it would be interesting to relate the order parameters in the two cases. While there is no local order parameter (local in $\tilde{\Lambda}$ basis) for distinguishing the small- α and large- α phases of Eq. 7, it is known to exist a two-dimensional membrane order parameter \tilde{O} [12]:

$$\tilde{O} = \left\langle \prod_{i \in \mathcal{C}} \tilde{\sigma}_i^x \prod_{i \in \mathcal{M}} \tilde{\sigma}_i^z \right\rangle \quad (11)$$

where \mathcal{C} refers to the four corners of a square membrane of one sublattice, and \mathcal{M} refers to all sites of the other sublattice which are enclosed by \mathcal{C} . It immediately follows that $\tilde{O} \mapsto O_{p,s}$, i.e. \tilde{O} can be mapped, according to Eq. 4, to the product of disconnected stabilizer operators as defined in Eq. 3, which serves as a natural order parameter of the FTC in Eq. 1. In particular, if \mathcal{C} in Eq. 11 is chosen to be the smallest possible membrane, i.e. that which contains only one site of the other sublattice, \tilde{O} would be mapped to a single A_p or B_s of the dual TC. Such correspondence between FTC and SSPT provides a lucid intuition for the topological nature of strong SSPT states, that the membrane order in SSPT cluster states is related to Abelian anyon excitations of a TC; or conversely, one may start from a TC model, where dressing an anyon operator with non-local string operators will give rise to a membrane topological order in SSPT cluster states.

Map to other strong SSPT models:- We have established a mapping from FTC to two copies of TPIM, as illustrated in Fig. 3(b) and (c). A natural question to ask is

if this insight would be useful in the construction of other SSPT models. Indeed, a lot of different 2D SSPT models have been proposed using symmetry defect homology theory [20]. The answer is affirmative. Here we give an example of mapping another frustrated TC model into the SSPT cluster model on a triangular lattice, whose Hamiltonian is generated by seven-qubit interactions as shown in Fig. 4(left). This model has strong SSPT order as is proved in Ref. [11]. Consider the following frustrated TC Hamiltonian that is different from Eq. 1:

$$H_{\text{FTC}_2} = -\sum_s A_s - \sum_p B_p + \alpha \sum_p \sigma_{1,p}^z \sigma_{2,p}^x \sigma_{3,p}^z \sigma_{4,p}^x + \alpha \sum_s \sigma_{1,s}^x \sigma_{2,s}^z \sigma_{3,s}^x \sigma_{4,s}^z \quad (12)$$

where the symbol $\sigma_{1,s(p)}^{z(x)}$ denotes the i -th spin in a plaquette or star. The index is increased clock-wisely and the bottom site is assumed to be $i = 0$. The perturbation term, up to a unitary rotation, is equivalent to an antiferromagnetic Xu-Moore model [24]. It does not commute with H_{TC} hence the topological order is again frustrated. For clarity we rewrite the perturbation term into

$$\sigma_{1,p}^z \sigma_{2,p}^x \sigma_{3,p}^z \sigma_{4,p}^x = -\sigma_{2,p}^y \sigma_{4,p}^y B_p \quad (13)$$

$$\sigma_{1,s}^x \sigma_{2,s}^z \sigma_{3,s}^x \sigma_{4,s}^z = -\sigma_{2,s}^y \sigma_{4,s}^y A_s \quad (14)$$

Applying the transformation in Eq. 4 to the right hand side gives us the cluster model defined on a triangular lattice, as is illustrated in Fig. 4. Other SSPT models with higher-order interactions can be generated by the same token, which we do not enumerate in the paper.

Relation to the plaquette Ising model:- To fully elucidate the physical understanding, it is imperative to investigate the relationship between the plaquette Ising model (PIM) [24, 35] and TC. Notably, a TPIM has been known to map onto two copies of PIM, leading to the designation of the former as the topological PIM (TPIM) [12]. To see the relation between TC and PIM and TPIM, consider the following Hamiltonian as an extended TC with additional “Y-checks”, which we shall refer to as YTC:

$$H_{\text{YTC}} = -\sum_s A_s - \sum_p B_p - \alpha \sum_s Y_s - \alpha \sum_p Y_p \quad (15)$$

Here we defined $Y_{s(p)} = \prod_{i \in s(p)} \sigma_i^y$, which does not commute with the A_s nor B_p . At small α , single anyon e , m and their fermionic bound states $e = e \times m$ are either completely immobile or partially mobile along lines, and only bosonic bound states $e_1 \times e_2$ or $m_1 \times m_2$ are completely mobile whose dispersion is again described by Eq. 2. This perturbation picture of anyon mobility is similar to the case of FTC, however, as we are to discuss, the YTC is mapped to PIM, instead of SSPT-ordered TPIM. Following the same map in Eq. 4, it is straightforward to see Eq. 15 is mapped to four copies of the

TABLE I. Variants of TC defined on Λ lattice (before transformation) and the effective model of its map in the $\tilde{\Lambda}$ lattice (after transformation)

$\sigma \in \Lambda$	$\tilde{\sigma} \in \tilde{\Lambda}$
TC	Paramagnet
TC with σ^y field	PIM
YTC (Eq. 15)	PIM $\times 4$
FTC (Eq. 1)	TPIM $\times 2$ (SSPT)
Half FTC (Eq. 10)	TPIM (SSPT)
FTC ₂ (Eq. 12)	Triangular cluster model (SSPT)

following terms

$$\mathcal{H}_\xi = -\alpha \sum_{\tilde{p}_\xi} \prod_{\tilde{p}_\xi} \tilde{\sigma}_{i \in \tilde{p}_\xi}^x - \sum_{i \in \tilde{\Lambda}_\xi} \tilde{\sigma}_i^z \quad (16)$$

where the subscript ξ in \tilde{p}_ξ and $\tilde{\Lambda}_\xi$ corresponds to the four distinct sublattices $\xi = 1, \dots, 4$ of $\tilde{\Lambda}$. This is the PIM that also enjoys a duality $\alpha \leftrightarrow \alpha^{-1}$, thus a transition at $\alpha = 1$. Indeed, as is discussed in [32, 33], a Zeeman field in σ^y would induce a single copy of PIM after the transformation, where there is no sublattice structure in $\tilde{\Lambda}$. Each sublattice Hamiltonian in Eq. 16 enjoys a subextensive number of Z_2 symmetries generated by $U_m^\xi = \prod_{n \in \text{cols}} \tilde{\sigma}_{m,n}^z$, $U_n^\xi = \prod_{m \in \text{rows}} \tilde{\sigma}_{m,n}^z$, with m, n are row and column indices bounded by the lattice size. A direct count yields a GSD for each pair of replicas equivalent to that of a TPIM, assuming the same lattice size characterized by either V or F .

We have explicated the relation between YTC and PIM, but what is the relation between YTC and FTC regarding the hidden SSPT phase in the later? Consider two of the four sublattices $\xi = 1, 2$, and define a non-local transformation: $\tilde{\sigma}_{i_1}^x = \tilde{\sigma}_{i_1}^x \prod_{i_2 \geq i_1} \tilde{\sigma}_{i_2}^z$, $\tilde{\sigma}_{i_2}^x = \tilde{\sigma}_{i_2}^x \prod_{i_1 \geq i_2} \tilde{\sigma}_{i_1}^z$, $\tilde{\sigma}_{i_{1(2)}}^z = \tilde{\sigma}_{i_{1(2)}}^z$, where $i_1 \in \tilde{\Lambda}_{\xi_1}$ and $i_2 \in \tilde{\Lambda}_{\xi_2}$. It is straightforward to check that under these transformation, the combination of the two copies in Eq. 16 becomes the TPIM Hamiltonian in Eq. 7 in $\tilde{\sigma}$ variables. Here one may immediately recognize that the YTC, as the mapped model of PIMs, can be converted to FTC, as the mapped TPIMs, by simply hitting all Y_s and Y_p operators in Eq. 15 by A_s and B_p . Hence the non-local transformation between TPIM and PIM in the dual lattices is achieved locally by applying canonical TC stabilizers, further establishing the deep relation between SSPT phases and the TC topological order. A summary of these mappings is presented in Table. I.

Discussion, conclusion and outlook:- Given the aforementioned mappings, we briefly comment on the differences between weak SSPT phases, which can be viewed as stacked or weakly coupled 1D SPT phases that retain their individual symmetries, and strong SSPT phases, which cannot be reduced to merely decoupled or weakly coupled 1D SPTs. It's useful to consider the hidden symmetry-breaking picture in SPT phases. Take for in-

stance a standard 1D SPT with $Z_2 \times Z_2$ symmetry and its corresponding non-local string order parameter. It is related to the symmetry-breaking picture of a hidden antiferromagnetic model after a non-local transformation [22, 23]. On the other hand, under the new mapping we introduced in Eq. 4, the TPIM can be mapped to two competing topological TC models in Eq. 1; or equivalently, a Half FTC-stabilizer model, corresponding to a set of mutually frustrating TC stabilizers; and the membrane order parameter associated with TPIM becomes a product of stabilizer operators in TC, underlining its intrinsic many-body nature as opposed to weak SSPT systems. This also makes explicit the fact that the SSPT-ordered TPIM model cannot be continuously deformed into a trivial phase in the thermodynamic limit, and the self-duality of TPIM is made manifestly clear in terms of the self-dual frustrated TC model. Interestingly, such connection not only exists between TPIM and TC model, but also holds for other SSPT models such as the triangular cluster model, which can emerge by inducing a different frustration on TC, hinting at a subtle linkage between topological order and strong SSPT order.

In summary, we have constructed exact maps connecting frustrated TC models to different SSPT-ordered models, showing that the novel SSPT phases of matter can be understood in terms of the simplest topological order in TC model. Given the rapidly evolving theories and experiments in quantum stabilizers and measurement-induced dynamics in various platforms [36–39], it is both theoretically and practically appealing that one may use the frustrated TC-stabilizer measurement to simulate SSPT phases and its fractonic dynamics, and construct equivalences of different SSPT models as dressed TC models. Conversely, one may also relate the engineering of quantum error correcting systems to SPT and SSPT phases. Since the TPIM model was originally proposed as a pathway to the one-way quantum computer [40, 41], it is intriguing to relate the measurement-based quantum computation to quantum error correction formalism. We believe that the above mapping which relates SSPT phase and the TC stabilizers is suggestive enough to warrant further studies.

Acknowledgement:- S. Feng acknowledges support from the Presidential Fellowship at The Ohio State University. S. Feng also thanks the Boulder Summer School 2023 at the University of Colorado Boulder for the enlightening lectures and discussions. Further gratitude is extended to X. Yang, N. Trivedi, A. Agarwala, and S. Bhattacharjee for their discussions and collaboration on related topics.

* E-mail: feng.934@osu.edu

[1] C. L. Kane and E. J. Mele, Z_2 topological order and the quantum spin hall effect,

Phys. Rev. Lett. **95**, 146802 (2005).

[2] I. Affleck, Quantum spin chains and the haldane gap, Journal of Physics: Condensed Matter **1**, 3047 (1989).

[3] F. Pollmann, E. Berg, A. M. Turner, and M. Oshikawa, Symmetry protection of topological phases in one-dimensional quantum spin systems, Phys. Rev. B **85**, 075125 (2012).

[4] X. G. Wen, Topological orders in rigid states, International Journal of Modern Physics B **04**, 239 (1990).

[5] X.-G. Wen, Colloquium: Zoo of quantum-topological phases of matter, Rev. Mod. Phys. **89**, 041004 (2017).

[6] X.-G. Wen, Quantum orders and symmetric spin liquids, Phys. Rev. B **65**, 165113 (2002).

[7] A. Kitaev, Anyons in an exactly solved model and beyond, Annals of Physics **321**, 2 (2006).

[8] Y. Zhou, K. Kanoda, and T.-K. Ng, Quantum spin liquid states, Rev. Mod. Phys. **89**, 025003 (2017), see also references therein.

[9] A. Y. Kitaev, Fault-tolerant quantum computation by anyons, Annals of Physics **303**, 2 (2003).

[10] X. G. Wen and Q. Niu, Ground-state degeneracy of the fractional quantum hall states in the presence of a random potential and on high-genus riemann surfaces, Phys. Rev. B **41**, 9377 (1990).

[11] T. Devakul, D. J. Williamson, and Y. You, Classification of subsystem symmetry-protected topological phases, Phys. Rev. B **98**, 235121 (2018).

[12] Y. You, T. Devakul, F. J. Burnell, and S. L. Sondhi, Subsystem symmetry protected topological order, Phys. Rev. B **98**, 035112 (2018).

[13] S. Vijay, J. Haah, and L. Fu, Fracton topological order, generalized lattice gauge theory, and duality, Phys. Rev. B **94**, 235157 (2016).

[14] H. Yan, Hyperbolic fracton model, subsystem symmetry, and holography, Phys. Rev. B **99**, 155126 (2019).

[15] H. Yan, Hyperbolic fracton model, subsystem symmetry, and holography. ii. the dual eight-vertex model, Phys. Rev. B **100**, 245138 (2019).

[16] W. Shirley, K. Slagle, and X. Chen, Foliated fracton order from gauging subsystem symmetries, SciPost Phys. **6**, 041 (2019).

[17] X.-G. Wen, Quantum orders in an exact soluble model, Phys. Rev. Lett. **90**, 016803 (2003).

[18] M. A. Levin and X.-G. Wen, String-net condensation: A physical mechanism for topological phases, Phys. Rev. B **71**, 045110 (2005).

[19] M. Levin and Z.-C. Gu, Braiding statistics approach to symmetry-protected topological phases, Phys. Rev. B **86**, 115109 (2012).

[20] N. Tantivasadakarn and S. Vijay, Searching for fracton orders via symmetry defect condensation, Phys. Rev. B **101**, 165143 (2020).

[21] T. Devakul, W. Shirley, and J. Wang, Strong planar subsystem symmetry-protected topological phases and their dual fracton orders, Phys. Rev. Res. **2**, 012059 (2020).

[22] T. Kennedy and H. Tasaki, Hidden $z_2 \times z_2$ symmetry breaking in haldane-gap antiferromagnets, Phys. Rev. B **45**, 304 (1992).

[23] T. Kennedy and H. Tasaki, Hidden symmetry breaking and the haldane phase ins=1 quantum spin chains, Communications in Mathematical Physics **147**, 431 (1992).

[24] C. Xu and J. E. Moore, Strong-weak coupling self-duality in the two-dimensional quantum phase transition of $p + ip$ superconducting arrays, Phys. Rev. Lett. **93**, 047003 (2004).

[25] W. Shirley, K. Slagle, and X. Chen, Foliated fracton order in the checkerboard model, Phys. Rev. B **99**, 115123 (2019).

[26] K. Slagle, Foliated quantum field theory of fracton order, Phys. Rev. Lett. **126**, 101603 (2021).

[27] J. P. Ibieta-Jimenez, L. N. Q. Xavier, M. Petrucci, and P. Teotonio-Sobrinho, Fractonlike phases from subsystem symmetries, Phys. Rev. B **102**, 045104 (2020).

[28] D. T. Stephen, A. Dua, J. Garre-Rubio, D. J. Williamson, and M. Hermele, Fractionalization of subsystem symmetries in two dimensions, Phys. Rev. B **106**, 085104 (2022).

[29] S. Trebst, P. Werner, M. Troyer, K. Shtengel, and C. Nayak, Breakdown of a topological phase: Quantum phase transition in a loop gas model with tension, Phys. Rev. Lett. **98**, 070602 (2007).

[30] J. Vidal, S. Dusuel, and K. P. Schmidt, Low-energy effective theory of the toric code model in a parallel magnetic field, Phys. Rev. B **79**, 033109 (2009).

[31] M. McGinley, M. Fava, and S. A. Parameswaran, Signatures of fractional statistics in nonlinear pump-probe spectroscopy (2022), arXiv:2210.16249 [cond-mat.str-el].

[32] S. Feng, A. Agarwala, S. Bhattacharjee, and N. Trivedi, Anyon dynamics in field-driven phases of the anisotropic kitaev model, Phys. Rev. B **108**, 035149 (2023).

[33] J. Vidal, R. Thomale, K. P. Schmidt, and S. Dusuel, Self-duality and bound states of the toric code model in a transverse field, Phys. Rev. B **80**, 081104 (2009).

[34] M. Mühlhauser, K. P. Schmidt, J. Vidal, and M. R. Walther, Competing topological orders in three dimensions, SciPost Phys. **12**, 069 (2022).

[35] C. Xu and J. Moore, Reduction of effective dimensionality in lattice models of superconducting arrays and frustrated magnets, Nuclear Physics B **716**, 487 (2005).

[36] A. Lavasani, Z.-X. Luo, and S. Vijay, Monitored quantum dynamics and the kitaev spin liquid (2022), arXiv:2207.02877 [cond-mat.str-el].

[37] A. Sriram, T. Rakovszky, V. Khemani, and M. Ippoliti, Topology, criticality, and dynamically generated qubits in a stochastic measurement-only kitaev model (2022), arXiv:2207.07096 [quant-ph].

[38] D. Bluvstein, H. Levine, G. Semeghini, T. T. Wang, S. Ebadi, M. Kalinowski, A. Keesling, N. Maskara, H. Pichler, M. Greiner, V. Vuletić, and M. D. Lukin, A quantum processor based on coherent transport of entangled atom arrays, Nature **604**, 451 (2022).

[39] N. Tantivasadakarn, A. Vishwanath, and R. Verresen, Hierarchy of topological order from finite-depth unitaries, measurement, and feedforward, PRX Quantum **4**, 020339 (2023).

[40] R. Raussendorf and H. J. Briegel, A one-way quantum computer, Phys. Rev. Lett. **86**, 5188 (2001).

[41] R. Raussendorf, D. E. Browne, and H. J. Briegel, Measurement-based quantum computation on cluster states, Phys. Rev. A **68**, 022312 (2003).